Prepared for submission to JINST

Particle Identification Algorithms for the PANDA Endcap Disc DIRC

M. Schmidt,[c,1] **A. Ali,**[a] **A. Belias,**[a] **R. Dzhygadlo,**[a] **A. Gerhardt,**[a] **K. Götzen,**[a] **G. Kalicy,**[a] **M. Krebs,**[a] **D. Lehmann,**[a] **F. Nerling,**[a] **M. Patsyuk,**[a] **K. Peters,**[a] **G. Schepers,**[a] **L. Schmitt,**[a] **C. Schwarz,**[a] **J. Schwiening,**[a] **M. Traxler,**[a] **M. Böhm,**[b] **W. Eyrich,**[b] **A. Lehmann,**[b] **M. Pfaffinger,**[b] **F. Uhlig,**[b] **M. Düren,**[c] **E. Etzelmüller,**[c] **K. Föhl,**[c] **A. Hayrapetyan,**[c] **K. Kreutzfeld,**[c] **O. Merle,**[c] **J. Rieke,**[c] **T. Wasem,**[c] **P. Achenbach,**[d] **M. Cardinali,**[d] **M. Hoek,**[d] **W. Lauth,**[d] **S. Schlimme,**[d] **C. Sfienti,**[d] **M. Thiel,**[d]

[a] *GSI Helmholtzzentrum für Schwerionenforschung GmbH, Darmstadt, Germany*
[b] *Friedrich Alexander-University of Erlangen-Nuremberg, Erlangen, Germany*
[c] *II. Physikalisches Institut, Justus Liebig-University of Giessen, Giessen, Germany*
[d] *Institut für Kernphysik, Johannes Gutenberg-University of Mainz, Mainz, Germany*

E-mail: mustafa.a.schmidt@physik.uni-giessen.de

Abstract: The Endcap Disc DIRC has been developed to provide an excellent particle identification for the future PANDA experiment by separating pions and kaons up to a momentum of 4 GeV/c with a separation power of 3 standard deviations in the polar angle region from 5° to 22°. This goal will be achieved using dedicated particle identification algorithms based on likelihood methods and will be applied in an offline analysis and online event filtering. This paper evaluates the resulting PID performance using Monte-Carlo simulations to study basic single track PID as well as the analysis of complex physics channels. The online reconstruction algorithm has been tested with a Virtex4 FGPA card and optimized regarding the resulting constraints.

Keywords: Cherenkov detectors, Particle identification methods

[1]Corresponding Author

Contents

1 Introduction

In the PANDA experiment, a cooled antiproton beam with a momentum up to 15 GeV/c collides with a fixed hydrogen target. The high luminosity annihilation and resulting particle creation processes allow to study fundamental questions in particle and hadron physics [1]. The Endcap Disc DIRC (EDD) is placed at the forward endcap of the PANDA target spectrometer and provides particle identification (PID) with a separation power of at least 3 standard deviation (s.d.) for $\pi^{\pm}$ and $K^{\pm}$ up to a particle momentum of $p = 4\,\mathrm{GeV/c}$.

Figure 1 illustrates the working principle of the EDD that consists of 4 independent quadrants. The left panel shows one of these quadrants that are made of a highly polished synthetic fused silica and 3×8 attached readout modules (ROMs). High momentum charged particles in PANDA, that penetrate the radiator plate, generate Cherenkov radiation. Most of the created photons are trapped inside the plate due to internal reflection and propagate to the ROMs, where the photon angles of internal reflection are measured. The radiator plate covers the polar angle range $5^{\circ} < \theta < 22^{\circ}$. Charged particles with smaller polar angles pass through the rhombic hole in the center of the radiator plate, and particles with larger polar angles will be shielded by the electromagnetic calorimeter [2].

Each ROM consists of 3 sensor elements containing a focusing element (FEL), that is bonded to a fused silica bar. The bar will be attached to the radiator quadrant with a special epoxy glue. A thin aluminum coating is applied on the backside of each FEL forming a cylindrical mirror. The internal reflected Cherenkov light travels from the point of intersection to the outer rim, where it enters one of the sensor elements and is being focused on the photocathode of an attached Multi Channel Plate Photo Multiplier Tube (MCP-PMT).

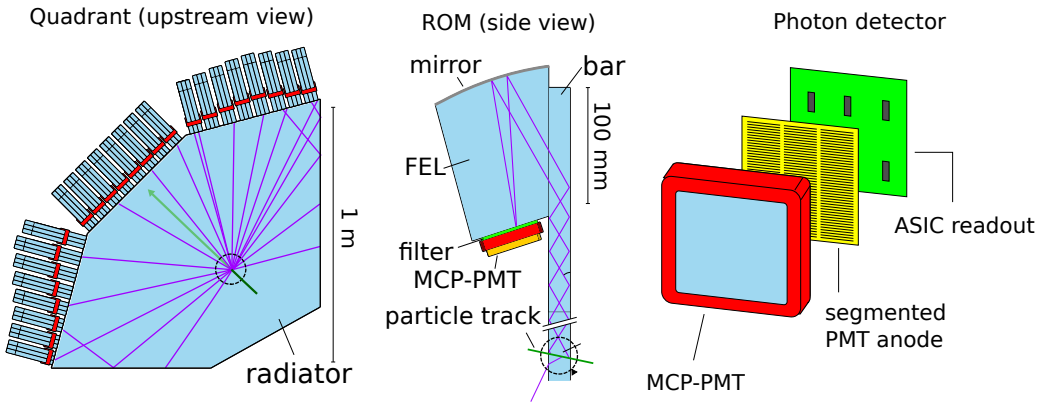

Figure 1. A sketch of one quadrant of the EDD (left) with 8 ROMs per side, the working principle of a sensor element (center) including the bar, FEL, and the MCP-PMT, and an exploded diagram of the attached MCP-PMT (right) with the segmented anode and the PCB of the ASIC readout.

The MCP-PMTs have a segmented anode with a fine granularity (3×100 or more strips). A fast ASIC readout system with a sufficient amount of channels is directly attached to the anode of the sensor, so the time information of every pixel can be read out individually. Optionally, an optical filter can be placed between the photocathode and the ROM surface in order to increase the Cherenkov angle resolution and detector performance by reducing dispersive effects. A detailed description of the setup and mechanical assembly can be found in [3].

2 Particle Identification

The EDD provides two spatial coordinates and a time stamp for each detected photon. The timing is used to separate Cherenkov photons from background hits. It is further used to distinguish between direct photons and those, which are reflected at the rim of the radiator plate. The two spatial coordinates in the MCP-PMT can be translated to a 2 dimensional angular information of the Cherenkov photon at the point of emission.

For the performance studies of the final detector, event based simulations have been performed. Thus, all primary charged particles are created independently from each other with a reseted initial time. From the stored time information of each hit, an average arrival time t_0, at which the particle enters the radiator plate, can be computed by theoretically calculating the propagation time of each photon inside the detector.

Two different methods are used to reconstruct the information about the particle types: The direct way, which is called *backward method*, calculates the Cherenkov angle that is assigned to each hit of a given charged particle track. In a second step the average of these angles is calculated and compared to a theoretically calculated Cherenkov angle for that given track and a given particle hypothesis. With the knowledge of the detector resolution this results in a likelihood value for a specific particle hypothesis, which is then used to calculate the particle probability. A more sophisticated procedure called *forward method* applies likelihood values to every pixel individually

by computing a theoretical hit pattern and estimating the error of every photon hit. Both methods are described in the following.

2.1 Geometrical Model

A geometrical model of the EDD, which has been introduced in [4], allows an analytical reconstruction and thus avoids implementation of large lookup tables. The definitions of the relevant angles are shown in Figure 2. The illustrated angle φ' in the sensor element can be directly calculated from the measured pixel position. It is connected to the angle φ between the photon trajectory related to the acquired hit and the surface of the radiator plate by the relation

$$\tan\varphi' = \frac{\tan\varphi}{\cos\alpha_{\mathrm{FEL}}} \tag{2.1}$$

where α_{FEL} is the angle between the photon trajectory and the orientation of the FEL. ϕ_{rel} is defined as the angle between the trajectories of the particle and the photon, and it is related to the azimuth angle of the charged particle.

For the geometrical reconstruction of the trajectory, the polar angle θ_p of the particle has to be known additionally. It is possible to show that the following equation can be used to reconstruct the Cherenkov angle of each photon hit in a direct and analytical way:

$$\theta_c = \arccos(\sin\theta_p \cos\phi_{rel} \cos\varphi + \cos\theta_p \sin\varphi) \tag{2.2}$$

In case of the forward method, the inverse calculation is required: The predicted angle φ has to be calculated according to

$$\cos\varphi = \frac{A\cos\theta_c}{B} \pm \sqrt{\frac{\cos^2\theta_p - \cos^2\theta_c}{B} + \left(\frac{A\cos\theta_c}{B}\right)} \tag{2.3}$$

with the values $A = \sin\theta_p \cos\phi_{\mathrm{rel}}$ and $B = A^2 + \cos^2\theta_p$. This equation is used to calculate a predicted hit pattern for each event and for different mass hypotheses by inserting the assumed Cherenkov angles θ_c for each mass hypothesis and the given track momentum.

2.2 Backward Method

The backward method is used to directly reconstruct the Cherenkov angle for each detected photon. By averaging over all photons of a single track, an average Cherenkov angle is obtained that can be compared with the theoretical Cherenkov angle according to

$$\cos\theta_C = \frac{1}{n\beta} \tag{2.4}$$

where β is calculated for all particle hypotheses. It is connected to the particle momentum according to the following relation:

$$\beta = \frac{p}{\sqrt{p^2 + m^2c^2}} \tag{2.5}$$

The momentum p has to be taken from the tracking information of PANDA. This reconstruction algorithm is faster than the forward method and therefore suitable for online event filtering processes.

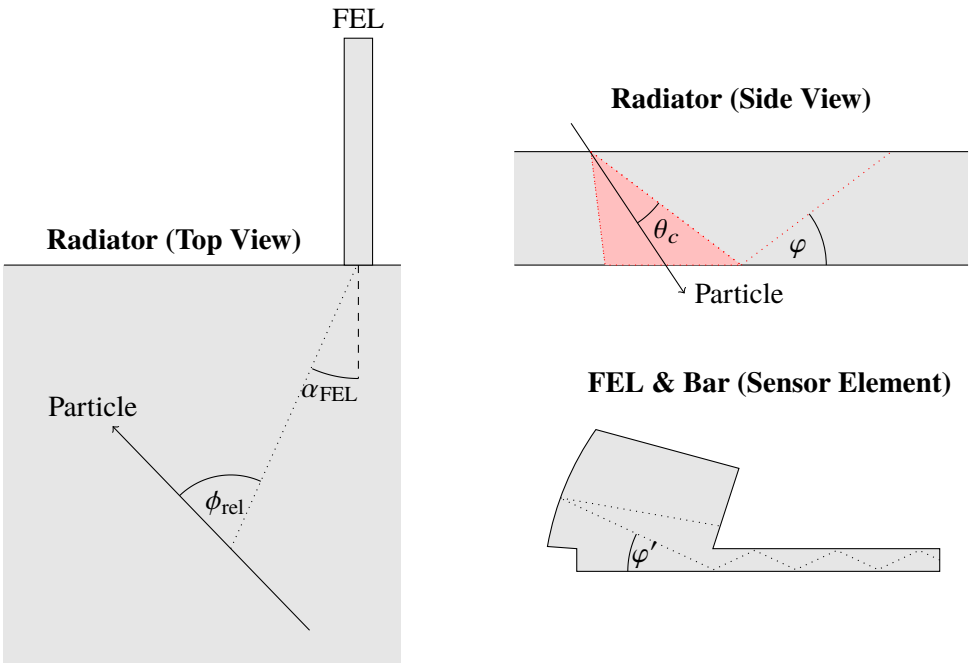

Figure 2. The angle definitions that are used for the reconstruction algorithm in the final EDD.

The refractive index n is obtained from an estimated average wavelength. Outliers in time are removed with an algorithm, that is based on the truncated mean method: For this reason, the propagation time of each photon has to be calculated according to

$$t = \frac{s}{v \cos \varphi} \tag{2.6}$$

where s is the distance between the intersection point and the FEL and v the group velocity inside the medium. By taking the relation with the speed of light into account, the propagation time can be written as

$$t_{ph} = \frac{s}{c \cos \varphi'} \left(n(\lambda) - \lambda \frac{\partial n(\lambda)}{\partial \lambda} \right) \tag{2.7}$$

After calculating a start time t_0, the hit with the largest time difference is deleted if it is larger than a given threshold. The best threshold value has been also obtained with the help of Monte-Carlo simulations. The truncation procedure continues until all outliers are removed and only hits in a given time window remain.

In order to get rid of the remaining background, hits with unphysical φ angles are additionally removed. This includes angles that cannot be created by the Cherenkov process or for which an internal reflection is not possible. For the calculation of a likelihood value, the average Cherenkov angle resolution has to be determined by Monte-Carlo simulations and is used as an input parameter for defining a normalized Gaussian density function.

Monte-Carlo results of reconstructed Cherenkov angles are shown in Figure 3. The left side shows a histogram with reconstructed Cherenkov angle for each photon hit individually, while the

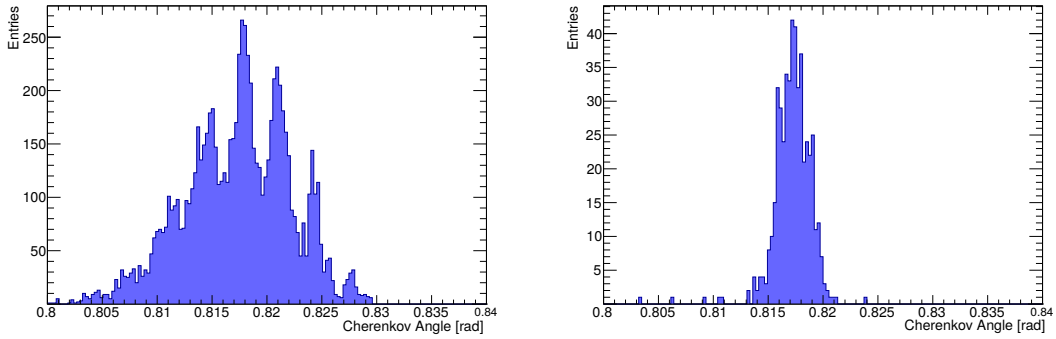

Figure 3. The single photon distribution for every hit (left) and the average Cherenkov angle distribution (right) for 1000 events with π^+ at a momentum of $p = 4\,\mathrm{GeV/c}$.

right histogram includes the Cherenkov angles that are averaged from all hits in one event. An average number of 21.2 hits per event has been obtained with Monte-Carlo simulations.

The resolution of the Cherenkov angle is obtained from the single photon resolution and the tracking detector resolution as follows:

$$\sigma_\theta^2 = \frac{\sigma_{\mathrm{ph}}^2}{N} + \sigma_{\mathrm{track}}^2 \tag{2.8}$$

The track resolution σ_{track} is a fixed value for every event and depends on the tracking system of PANDA. However, the photon resolution σ_{ph} is a function of the geometrical and chromatic error of the detector and is scaled therefore by a factor $\sqrt{N}$ for the detection of N photon hits per event. Hence, a higher photon statistics results in a better performance.

2.3 Forward Method

The forward method is used for the offline analysis only, because it would be too slow for an online event filtering. In this method, the tracking information and the mass hypotheses for the particles, that have to be taken into account, are used to calculate a predicted hit pattern for each hypothesis. These predicted hit patterns are compared to the measured hit pattern. They contain the pixel information, the FEL number, and the time information.

In the first step, a coarse spatial cut is applied by removing outliers in the pixel space that are not located inside a given pixel window around at least one calculated hit. One possibility for avoiding a spatial cut is the assumption of background hits, resulting in an offset of the Gaussian distribution. This offset is used to suppress data points that are located too far away from the predicted hit. The correct amount of background hits has been obtained from Monte-Carlo simulations.

For the pattern matching algorithm, all additional photon reflections on the outer rim have to be taken into account. The calculation of the reflected hit patterns is done by mirroring the particle trajectory on each of the quadrant sides and compute a virtual point of intersection that is placed outside of the quadrant. A truncated mean algorithm for removing unwanted outliers is implemented in this method.

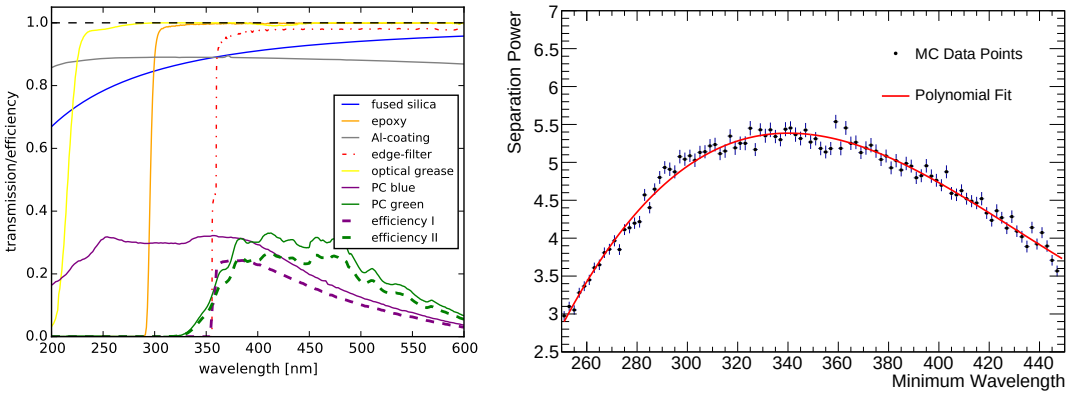

Figure 4. The optical parameters implemented inside the Monte Carlo simulations (left) and the simulated detector resolution as a function of the minimum wavelength of the band-pass filter (right).

For every remaining hit i a likelihood value can be computed by assuming a Gaussian probability distribution for the spatial and time information. The sum of the logarithmic likelihood values can then be written as follows:

$$\ln \mathcal{L} = \sum_{i=0}^{N} \left(\ln \mathcal{G}(z_i | z_{\text{pred},i}; \sigma_z) + \ln \mathcal{G}(t_i | t_{\text{pred},i}; \sigma_t) \right) \tag{2.9}$$

The errors σ_t depend on the readout resolution, σ_z includes the chromatic and geometrical errors and can be calculated analytically by using the method of error propagation in combinations with the equations given above. It turned out that several simplifications with only a minor effect on the detector performance could be applied in order to decrease the number of mathematical terms that have to be computed.

2.4 Performance Analysis

The Monte-Carlo simulations have been performed with the PandaRoot framework [5], that has been designed for the data analysis of PANDA and also includes a simulation part based on Virtual Monte Carlo (VMC). VMC is implemented in ROOT and uses the Geant4 transport algorithms.

An updated geometry of the EDD with 8 ROMs per side has been designed and implemented in the simulation part of PandaRoot. Additionally, all optical parameters like the wavelength dependent refractive index of fused silica and the detection efficiency of the attached MCP-PMTs are used for a full simulation of one detector quadrant as displayed in left tile of Figure 4. The detector performance has been studied for two different types of photocathodes: a standard *blue photocathode* with a large plateau between 250 nm and 400 nm and a *green photocathode* with a rising edge around 250 nm and an enhanced quantum efficiency in the green spectrum. The collection efficiency has been set to a constant value of 65 %.

The optimum for the minimum wavelength of the used band-pass filter to minimize chromatic errors has been studied with the help of Monte-Carlo simulations. It has turned out that the best detector performance regarding the separation power can be obtained for a cut-off value around

340 nm as presented on the right side of Figure 4. This plot shows the separation power between $\pi^{\pm}$ and $K^{\pm}$ as a function of the minimum wavelength of the band-pass filter. The upper wavelength limit of the band-pass filter is placed above the detection efficiency region of the MCP-PMTs. The obtained wavelength for the maximum separation power has then been used for all further simulation studies.

The digitization part in PandaRoot converts the hit coordinate on the MCP-PMT photocathode and the time information from the Monte Carlo data into discrete pixel positions and time stamps with a binning of 50 ps. In addition, a Gaussian time smearing with a s.d. of $\sigma = 30$ ps for every hit is applied. This value has been adapted to the specifications of the TOFPET ASIC [6] which is the chosen readout for the final detector.

For the reconstruction part, the Monte Carlo truth data of the charged particle including the position and angle information on the radiator plate has been used and a Gaussian smearing to simulate the influence of the PANDA tracking resolution has been applied. The reconstruction algorithms are applied for pion and kaon mass hypotheses and the separation power is calculated from the differences of the likelihood values of both particle species.

As described above, all quadrants are independent from each other. Hence, only one quadrant has been chosen for the performance analysis. The simulated detector resolution for a fine binning on the radiator plate is presented on the left side of Figure 5. The π^{+} and K^{+} are created with a uniform distribution of the polar and azimuth angle at the target position. The VMC engine propagates them in the presence of a magnetic field, that is given in the form of a field map as an input parameter, on a helix trajectory to the surface of the radiator plate. The binning of the particle position is taking place during the reconstruction phase.

These simulation studies show that the separation power reaches values up to 6 s.d. for small polar angles. As anticipated from theoretical calculations, the detector performance decreases for larger polar angles due to a larger influence of the geometrical error which cannot be compensated by the higher amount of detected hits. The values for particles with polar angles larger than 22° have been filtered out, since these tracks will be accepted and identified by the PANDA Barrel DIRC detector.

Another effect can be seen for small azimuth angles on the lower side of the radiator quadrant where the separation power drops due to an overlap of the hit patterns of the direct and reflected photons. In this area, the differences between the time stamps get close to the time resolution of the readout system. As a result, the hit patterns cannot be distinguished any more and the performance deteriorates. However, for very small distances between the particle and the rim, the separation power increases again as one can see in the 2 dimensional representation. For particles with lower momenta, the area of the deteriorated separation power shifts to larger azimuth angles due to the influence of the magnetic field. The asymmetry comes from the bending of the particle trajectory in the magnetic field.

A projection of the separation power as a function of the polar angle θ of the particle can be seen on the right hand-side of Figure 5 for different momenta and both analyzed photocathodes. The analysis shows a sufficient particle separation for all relevant polar angles. The setup including the green photocathode guarantees a slightly better performance over the whole polar angle range.

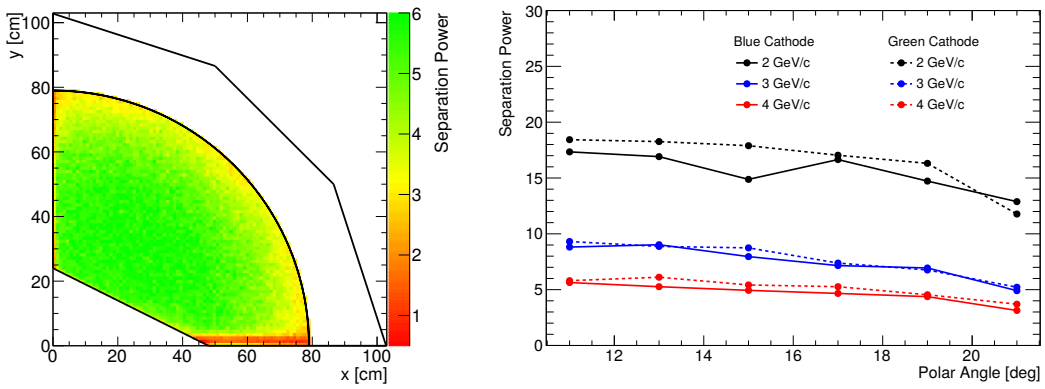

Figure 5. The detector resolution for all relevant positions on the radiator plate for a particle momentum of $p = 4\,\mathrm{GeV/c}$ (left) and the projected separation power as a function of the polar angle for different particle momenta (right).

2.5 Physics Channel Analysis

As performance study of the EDD, a specific physics channel has been chosen. It consists of the two decay branches

$$\bar{p}p \rightarrow f_0\pi^0 \rightarrow K^+K^-\pi^0 \tag{2.10}$$

$$\bar{p}p \rightarrow f_0\pi^0 \rightarrow \pi^+\pi^-\pi^0 \tag{2.11}$$

$$\tag{2.12}$$

including the decay of the glueball candidate $f_0(1500)$ [7] into two kaons with a probability of approx. 4.3% and two pions with a probability of 23.3%. The latter is used as one possible background channel for studies regarding misidentification. These decay branches are implemented in the event generator of the PandaRoot framework.

The tracking algorithms in PandaRoot provide the reconstructed position and momentum information of all particles, that are related to one event. A self-written helix propagator has been used to propagate the charged particles from the last point of reconstruction to the surface of the radiator disk by assuming a constant magnetic field in this area. By including all PID detectors, a global likelihood value for every reconstructed track in each event can be computed.

From the general notation of the Bayes' theorem

$$p(\theta|x) = \frac{\mathcal{L}(\theta|x)\pi(\theta)}{\int \mathcal{L}(\theta'|x)\pi(\theta')d\theta'} \tag{2.13}$$

the probability for the particle hypothesis k can be derived. The a-priory probability $\pi(\theta)$ has been set to in order to create comparable results. This parameter is equal to an assumed probability of the charged particle to enter one specific sub detector. The probability is then being calculated as

$$p(k) = \frac{\prod_i \mathcal{L}_i(k)}{\sum_j \prod_i \mathcal{L}_i(j)} \tag{2.14}$$

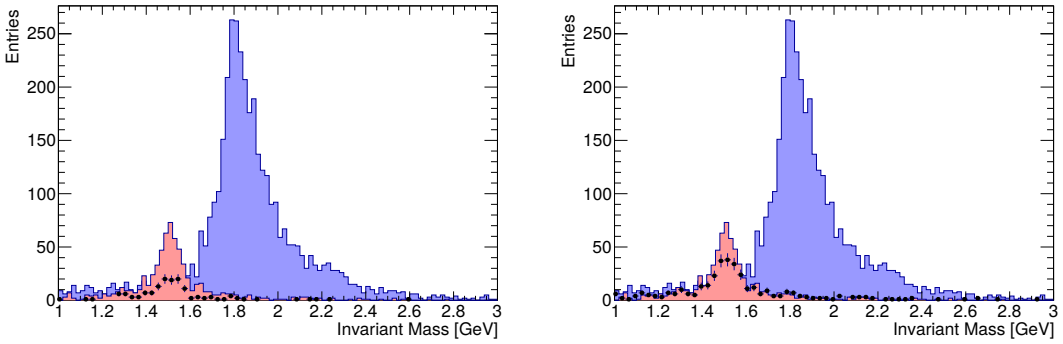

Figure 6. The reconstructed rest mass of the $f_0(1500)$ particle excluding (left) and including (right) the EDD. The blue histogram shows the events with created pions, and the red entries represent the events including a decay into two kaons. The dots with error bars represent the events where the decay products are identified as kaons.

where i is the index of the sub detector and j one of the 5 particle hypotheses e, μ, π, K, p. These sub-detectors excluding the EDD are namely the Straw Tube Tracker (STT), Micro Vertex Detector (MVD), the PANDA Muon Range System including the Mini-Drift Tubes (MDT), and the Barrel DIRC.

The left side of Figure 6 shows the calculated invariant mass m_0 of the f_0 without using the PID information from the EDD, while the right hand side presents the results including the EDD. The blue entries represent the rest mass with the momentum information of π^+/π^- events before applying PID, while the red histograms show the mass reconstruction with K^+/K^- events. The points with error bars in both histograms indicate the amount of events that are identified as K^+/K^- events. The analysis shows, that inserting the EDD leads to a 58% higher signal-to-background ratio compared to a PANDA spectrometer without it.

3 Online Reconstruction

3.1 Experimental Setup

An online reconstruction tool used for feasibility studies has been written in VHDL and tested with an ML403 board containing a Xilinx Virtex4 FPGA chip. The fast gigabit Ethernet communication is handled by the library package SiTCP [8] that has been developed at KEK. This package is limited to a small group of existing FPGA boards. The used ML403 contains 632 kB RAM and together with the SiTCP package a frequency of 120 kHz can be achieved. For testing the online reconstruction algorithm, the data has been sent by a network client software via an Ethernet connection to a first in, first out (FIFO) buffer provided by SiTCP. It has to be taken into account that the FIFO buffer can only process 8-bit integers in one clock cycle. Therefore, larger fixed point numbers have to be divided in smaller blocks before transmitting them to the FPGA card.

The online reconstruction algorithm is tested with Monte-Carlo data created in PandaRoot. A self-written terminal application is used to transmit the fixed point numbers of the particle track and

hit pattern information via a network cable to the FIFO buffer. With every clock cycle one integer value can be read from the FIFO buffer and processed by the implemented routines.

The board limitations constrain the possible approaches for reconstruction algorithms. All relevant angles can be evaluated with trigonometric functions which makes the computation of dot products and square roots essential. Lookup tables in the form of array functions $(1,0)^n \rightarrow (1,0)^m$ consume $m \cdot 2^n$ bits of memory. Table 1 presents the required memory as a function of the fixed point resolution.

Array Size	Memory Requirement
8 bit	256 B
16 bit	128 kB
32 bit	16 GB

Table 1. The memory consumption of lookup tables for different integer sizes.

3.2 Online Reconstruction Algorithm

In order to avoid memory problems, the Coordinate Rotation Digital Computer (CORDIC) algorithm has been used [9] for numerical computations. It calculates the sine and cosine values of an angle θ by rotating the unit vector $(x0, y0) = (1, 0)$ with the rotation matrix

$$\begin{pmatrix} x_1 \\ y_1 \end{pmatrix} = \begin{pmatrix} \cos\theta & -\sin\theta \\ \sin\theta & \cos\theta \end{pmatrix} \cdot \begin{pmatrix} x_0 \\ y_0 \end{pmatrix} \tag{3.1}$$

The trigonometric functions can be exchanged with the tangent value of θ. By using the linear combination of θ with small angles α_i and exchanging the resulting tangent function with $\tan\alpha_i = 2^{-i}$, the small rotations can be written as the following product of matrices:

$$\begin{pmatrix} x_n \\ y_n \end{pmatrix} = K \prod_{i=0}^{n} \begin{pmatrix} 1 & -\sigma_i \cdot 2^{-i} \\ \sigma_i \cdot 2^{-i} & 1 \end{pmatrix} \cdot \begin{pmatrix} x_i \\ y_i \end{pmatrix} \tag{3.2}$$

where σ_i stands for the signum function and can take the values $+1$ and -1. The binary shifting with powers of 2 is ideal for calculations on an FPGA card. The amplitude factor is given by

$$K = \prod_{i=0}^{n-1} \frac{1}{\sqrt{1 + 2^{-2i}}} \tag{3.3}$$

which converges to a constant value.

This method requires only one lookup table for the arcus tangent, that can be implemented with a high resolution. A parallel implementation of the CORDIC algorithm can reduce the latency for every calculation step down to 2 clock cycles while a serial implementation needs less resources and allows pipelining if necessary. The disadvantage is then the longer latency with more than 10 clock cycles depending on the integer resolution.

With minor modifications this algorithm can be further used for the computation of square roots and hyperbolic functions. The results of the reconstructed Cherenkov angle for pions and

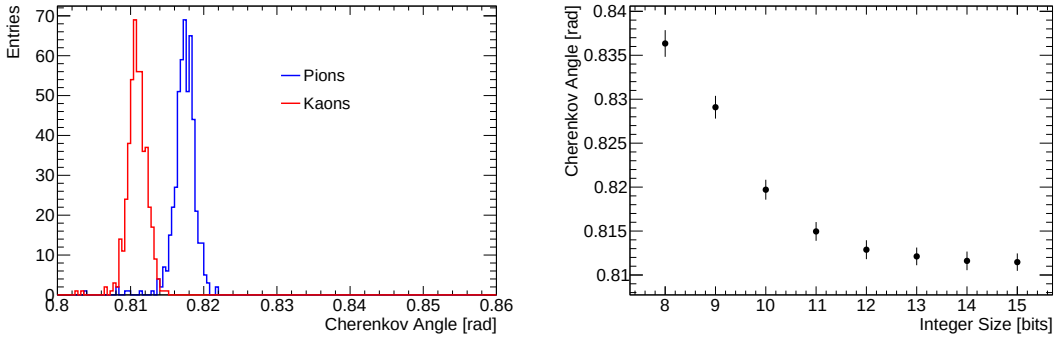

Figure 7. Reconstructed average Cherenkov angle per event for pions and kaons with 16-bit integer resolution (left) and the Cherenkov angle offset as a function of the fixed point resolution. The resolution is illustrated by the error bars.

kaons with a momentum of $p = 4\,\text{GeV/c}$ and a polar angle of $\theta = 12°$ are presented in Figure 7. The results show a large offset of the reconstructed average Cherenkov angle for a coarse resolution of 8-bit and a resolution that would not be sufficient for an online event filtering.

The analysis proves further, that using a resolution larger than 16-bit is sufficient for the desired detector performance, and reduces the influence of the fixed point resolution to a negligible value. The number of clock cycles that are needed for processing one single hit could be reduced to 10. In contrast to this, numerical calculations with a lookup table can provide the results instantly, but consume a higher amount of memory.

4 Conclusion & Outlook

The detector performance study has been used to validate the detector geometry and used components with respect to the requirements of PANDA. The implemented particle identification algorithms and the actual detector design ensure a minimum of 3 s.d. separation power over the whole polar angle range. It has been proven that the two investigated photocathodes of the MCP-PMTs are providing similar results. This can make the original planned filter obsolete leading to a simpler and cost optimized detector setup.

The production of a glue ball has been used for a benchmark channel analysis showing promising results. A deeper analysis with more background channels using the dual parton model (DPM) generator is ongoing. In a feasibility study, the online reconstruction has been implemented on a sample FPGA board. As a next step it is planned to build a full size Disc DIRC quadrant, and to evaluate its performance in a cosmics test stand as well as in the PANDA detector.

References

[1] F. Iazzi, *The panda physics program: Strangeness and more*, *AIP Conference Proceedings* **1743** (2016) 050006, [http://aip.scitation.org/doi/pdf/10.1063/1.4953307].

[2] PANDA collaboration, W. Erni et al., *Technical Design Report for PANDA Electromagnetic Calorimeter (EMC)*, 2008. 0810.1216.

[3] E. Etzelmüller, *Developments towards the technical design and prototype evaluation of the PANDA Endcap Disc DIRC*. PhD thesis, University of Giessen, Gießen, 2017.

[4] O. Merle, *Development, design and optimization of a novel Endcap DIRC for PANDA*. PhD thesis, University of Giessen, 2014.

[5] S. Spataro and the PANDA Collaboration, *The PandaRoot framework for simulation, reconstruction and analysis*, *Journal of Physics: Conference Series* **331** (2011) 032031.

[6] M. D. Rolo, R. Bugalho, F. Goncalves, G. Mazza, A. Rivetti, J. C. Silva et al., *TOFPET ASIC for PET applications*, *Journal of Instrumentation* **8** (2013) C02050.

[7] P. Minkowski and W. Ochs, *The J**PC = 0++ scalar meson nonet and glueball of lowest mass*, in *Hadron spectroscopy. Proceedings, Workshop, Frascati, Italy, March 8-12, 1999*, pp. 245–255, 1999. hep-ph/9905250.

[8] T. Uchida, *Hardware-based tcp processor for gigabit ethernet*, *IEEE transactions on nuclear science* **55** (jun, 2008) 1631–1637.

[9] J. E. Volder, *The CORDIC Trigonometric Computing Technique*, *IRE Transactions on Electronic Computers* **EC-8** (Sept, 1959) 330–334.